Journal of Constructional Steel Research 198 (2022) 107499

Contents lists available at ScienceDirect

Journal of Constructional Steel Research

journal homepage: www.elsevier.com/locate/jcsr

Mechanical properties of butt-welded ultra-high strength steels at elevated temperatures

Mehran Ghafouri [a], Mohsen Amraei [b,*], Aki-Petteri Pokka [c], Timo Björk [a], Jari Larkiola [c], Heidi Piili [b], Xiao-Lin Zhao [d]

[a] Laboratory of Steel Structures, School of Energy Systems, LUT University, P.O. Box 20, 53851 Lappeenranta, Finland
[b] Department of Mechanical and Materials Engineering, University of Turku, Turku 20520, Finland
[c] Materials and Production Engineering, Faculty of Technology, University of Oulu, P.O. Box 4200, 90570 Oulu, Finland
[d] Department of Civil and Environmental Engineering, The Hong Kong Polytechnic University, Hong Kong, China

ARTICLE INFO

Keywords:
Ultra-high strength steel
Welded joints
GMAW
Mechanical properties
Elevated temperature
Fire-resistance design

ABSTRACT

Variety of ultra-high strength steels (UHSS) with different microstructural characteristics is becoming available with continuous development of the manufacturing process in the steel industries. In order to effectively design structures made of such steel grades, a detailed knowledge of the mechanical properties is vital. Fire safety design is one of the areas in which such knowledge is essential. Welding process is indispensable in construction of steels structures with inevitable welding-induced degradation of mechanical properties of UHSSs. Thus, conducting experimental research on elevated-temperature constitutive mechanical behavior of welded joints made of UHSSs is of paramount importance. This study addresses elevated-temperature mechanical properties of as-received and as-welded S960 (manufactured via direct quenching technique) and S1100 (quenched and tempered) steel grades. A fully automated gas metal arc welding (GMAW) process with low heat input value was utilized to join the steel plates. Next, steady-state uniaxial tensile tests in the temperature range between room temperature (RT) and 900 °C were carried out. Accordingly, reduction factor-temperature relations for each tested steel in both as-received and as-welded forms are discussed and compared with several design standards, as well as with previous studies in the literature. Finally, predictive equations are proposed to estimate the elevated-temperature mechanical properties reduction factors of the tested UHSSs in as-received and as-welded forms.

1. Introduction

Steels with different degrees of strength have been used during the past decades in various applications, such as the automotive industry, construction of large-span bridges, and skyscrapers all around the globe. Less exploitation of natural resources and energy-saving trends in recent years from one side and demand of fast-growing technology from the other side have triggered the invention and development of high and ultra-high strength steels (HSS/UHSS). These materials offer a superb combination of load-bearing capacity and high strength-to-weight ratio combined with good weldability, which makes them highly useful in a variety of industrial applications [1–5]. In the field of construction and structural engineering, application of HSS and UHSS can lead to environmental and socioeconomic benefits: decreasing material consumption via obtaining smaller cross-sectional size in design, saving labor and costs related to fabrication and transportation, as well as reducing carbon emission [3,6].

In the field of construction, fusion welding processes and particularly conventional arc welding techniques have been frequently applied to make permanent joints between structural members and components made of UHSSs due to their cost-effectiveness, versatility and reliability [7–9]. However, since UHSS is manufactured in a controlled heating and cooling process resulting in a certain microstructural characteristic, the welding thermal cycles can deteriorate the desired microstructure [10]. The research on welded UHSS is mainly focused on GMAW [11,12] and laser welding (LW) [10,13]. Some detrimental phenomena are attributed to tremendous heat input from the welding processes (GMAW for example has higher level of heat input compared to LW), such as strength reduction (under fatigue and tensile loads) due to the softened heat-affected zone (HAZ). Skriko et al. [14] found that TIG-dressing of T-

* Corresponding author.
E-mail address: Mohsen.amraei@utu.fi (M. Amraei).

https://doi.org/10.1016/j.jcsr.2022.107499
Received 19 May 2022; Received in revised form 6 August 2022; Accepted 9 August 2022
Available online 9 September 2022

joints made of S960 causes significant softening in the fusion line and HAZ, which has negative effects on fatigue strength of the joint. According to the literature, the tensile strength reduction at the softened HAZ can reach as high as 60% [10,13,15,16]. Hence, great attention should be paid to the design of welded connections made of UHSSs.

Fire can be mentioned as among the most, if not the most, prominent catastrophic incidents to which structures are vulnerable, which can result in structural failure, followed by extreme consequences such as human fatalities, economic loss and environmental pollution [4,6,17–20]. Fire-safe designs and assessing the performance of steel structures made of HSSs and UHSSs exposed to fire conditions necessitate a profound understanding of constitutive behavior of such materials at elevated temperatures. Numerous research efforts have been hitherto conducted to investigate the mechanical properties of steels at elevated temperatures and post-fire mainly on mild steels [21,22].

Existing models in leading design standards such as Eurocode 3 (EC3) [23] for constitutive behavior of steels at elevated temperatures are generally based on reduction factors for mechanical properties including elastic modulus, yield strength and ultimate tensile strength. These models, however, have been developed based on the results for mild steels, and adoption of those code models for estimating the mechanical properties of HSSs and UHSSs at elevated temperatures is still questionable. Due to lack of recommendations for HSSs and UHSSs in the current design codes and urgent need for assessing the degradation of mechanical properties of HSSs and UHSSs in fire and post-fire conditions, several research studies have been conducted [4,6,17,24–28]. Qiang et al. [26] studied mechanical properties of S960QL (manufactured via quenched and tempered process) in fire conditions by conducting steady and transient hot tensile tests in the temperature range 20–700 °C. Characteristic strengths obtained from their tests were compared with different leading design standards. Their results revealed that none of the proposed models by design codes can be used for accurate prediction of mechanical properties of their UHSS at elevated temperatures. They concluded that degradation of mechanical properties of HSSs and UHSSs at elevated temperatures is contingent upon steel grade and manufacturing process. Neuenschwander et al. [4] conducted extensive comparative research on deterioration of mechanical properties of S690QL and S960QL at different strain rates under steady-state and transient conditions at temperatures 20 °C–900 °C. Comparing their results in the case of HSSs with grades below S700 with EC3, they showed that the Eurocode predictive model for elastic modulus and effective yield strength at 2% total strain at elevated temperatures is overconservative and nonconservative, respectively. For UHSSs with grades above S700, they noted the necessity of more experimental research to conclusively assess the adoptability of the EC3 model for prediction of mechanical properties at elevated temperatures.

Although there has been some research on deterioration of mechanical properties of HSSs and UHSSs at elevated temperatures in the context of fire-safe designs, only a few studies focused on steel grades above 900 MPa [4,26,29,30]. These researchers, however, conducted their experiments on quenched and tempered UHSSs; direct-quenched steels were not included in their investigations. As has been reflected in the literature [17], mechanical properties of UHSSs at elevated temperatures are highly dependent on chemical composition, especially carbon content and manufacturing process, which necessitates conducting research on UHSSs with different manufacturing processes. More importantly, elevated-temperature mechanical properties of welded joints made of UHSSs have not been investigated thus far. Inasmuch as welding is indispensable in construction of steel structures, and degradation of mechanical properties of UHSSs is inevitable due to welding [10], conducting experimental research on elevated-temperature constitutive mechanical behavior of welded joints made of UHSSs is of paramount importance. Such research contributes to provide scientific background to improve code models and scrutinize the suitability of adopting those predictive models for UHSSs.

This study fills the knowledge gap in understanding elevated-temperature mechanical properties of as-received and as-welded ultra-high strength steel by including two UHSSs not covered in the literature, namely S960MC (manufactured via direct quenching technique) and S1100 (quenched and tempered) steel grades. In this regard, four sets of specimens were prepared, and steady-state tensile tests in the temperature range RT–900 °C were carried out. For each specimen elastic modulus, effective yield strength at 0.2% strain level and ultimate tensile strength are obtained from stress-strain curve at corresponding temperature. Accordingly, reduction factor-temperature relations for each tested steel in both as-received and as-welded forms are discussed and compared with some leading design standard predictive models, such as the EC3, the American Institute of Steel Construction (AISC) [31], and the Australian Standard AS4100 [32]. Moreover, comparison of the results with the existing literature for different grades of HSS/UHSSs, such as S460N (normalized rolled delivery condition) [33], S700MC (thermomechanically rolled delivery condition) [17] and S960QL [4,26] is also performed. Finally, this paper further extends the knowledge through establishing predictive equations to safely estimate the elevated-temperature elastic modulus, 0.2% proof stress, and ultimate tensile strength reduction factors of the tested steels in both as-received and as-welded forms. In addition, comparisons between the proposed equations and the above-mentioned design code models are drawn.

2. Materials and experimental procedure

2.1. Materials

The base materials (BMs) considered for this study were S960MC and S1100 UHSS alloys with low carbon contents. As-received S960MC was manufactured by modern hot rolling and direct quenching processes [34], while the S1100 grade was manufactured by the quenching and tempering process [16]. Both steel alloys were received from 8 mm thick hot rolled strips. The chemical compositions (wt%) of the two steel grades according to the manufacturer's certificates are listed in Table 1.

The carbon equivalent *(CEV)* in Table 1 is calculated using the following equation:

$$CEV = C + \frac{Mn}{6} + \frac{Cr + Mo + V}{5} + \frac{Ni + Cu}{15} \quad (1)$$

The nominal mechanical properties of the studied steels are presented in Table 2.

The effects of elevated temperatures on the constitutive mechanical properties (i.e. elastic modulus, 0.2% proof and ultimate tensile stress) of butt-welded UHSSs were studied in this paper. The GMAW process which is commonly used to join UHSSs, was applied to achieve this aim [10,35]. Due to softening effect at the weld HAZ, especially in direct-quenched (DQ) UHSSs, welding parameters were chosen so that heat input (HI) level falls in an optimum range as recommended in the literature [10,36]. The specimens were allowed to cool down to room temperature between each weld pass. Similar welding parameters were utilized for both steel alloys as shown in Table 3. In order to achieve high quality and consistency in welding, a fully automated process using a robot arm was used.

The applied HI due to the welding was calculated according to Eq. (2):

$$Q = U \times I \times \eta / (\nu \times 1000)\ (kJ/mm) \quad (2)$$

where Q is heat input, U voltage, I electric current, η welding efficiency coefficient, and ν travel speed of the welding torch. Considering a welding efficiency coefficient of 0.8 for the GMAW process, a net HI value of 0.7 kJ/mm was calculated, which lies in the permitted range for the two steel grades.

The filler material used in the GMAW process was Böhler Union X96 solid wire. The nominal yield and ultimate tensile strength of the filler

Table 1
The nominal chemical composition of BMs (wt%).

Steel	C	Si	Mn	P	S	V	Cu	Cr	Ni	Mo	CEV
S960	0.088	0.2	1.11	0.008	0.000	0.010	0.009	1.09	0.06	0.125	0.52
S1100	0.129	0.18	1.48	0.006	0.002	–	0.439	1.29	0.99	0.371	0.83

Table 2
Nominal mechanical properties of the parent materials.

Steel	Min 0.2% proof strength (MPa)	Ultimate tensile strength (MPa)	Elongation A_5 (%)
S960	1028	1126	9
S1100	1126	1153	11

Table 3
Welding parameters used in the experiment.

Voltage (V)	Current (A)	Travel speed (mm/s)	Wire feed rate (m/min)	Wire diameter (mm)	Gas flow (L/min)	Shielding gas
25.1	216	6.2	10	1.0	20	92% Ar + 8% CO_2

material are slightly lower than those of parent materials. However, previous studies prove the strength of the welded joints made from both steels falls in the matching strength level with the BMs [10]. Table 4 lists chemical composition (wt%) as well as the mechanical properties of the filler material used in this study.

The microstructure of both steel grades is a mixture of bainite (B), martensite (M), islands of martensite/austenite (M/A) and tempered martensite as shown in Fig. 1. The details of the microstructure of the BM studied in this paper can be found at [10,16]. The low carbon content makes these steel grades suitable for welding, hence their potential for construction applications. However, the martensitic microstructure of these steel grades is more sensitive to the welding HI, hence softening at the weld HAZ may occur [37]. In order to overcome this issue, the welding HI should be kept as low as possible [10].

2.2. Test specimens

Two sets of specimens for each steel grade (i.e. as-received and as-welded) were manufactured according to the specifications of ASTM E8M [38]. Due to thickness limitations, sub-sized specimens were made. At first, 8 mm thick steel plates were laser cut in rolling direction. Then, the cut pieces were machined to form cylindrical specimens as shown in Fig. 2. Due to the limitation in fixtures at elevated temperatures, cylindrical shape was chosen.

In order to manufacture as-welded specimens, two laser-cut base plates were butt-welded using a robot arm from which the samples were cut. Hence, all specimens were taken from the welded block as shown schematically in Fig. 3. Prior to groove preparation, edges at the weld area were removed mechanically for 2 mm to eliminate possible HAZ from the laser cutting process. The double V-shape groove was then prepared by machining. The schematic of the joint is shown in Fig. 3(a). After welding, specimens were laser cut from the welded workpiece perpendicular to welding direction (parallel to rolling direction) as shown schematically in Fig. 3(b). Sectioned specimens were machined to produce cylindrical specimens identical to those from BM in accordance to the specification of ASTM E8M [38].

Table 4
Chemical composition (wt%) and nominal mechanical properties of Union X96.

	C	Si	Mn	Cr	Mo	Ni
	0.12	0.8	1.90	0.45	0.55	2.35
Union X96	Yield Strength (MPa)		Ultimate tensile strength (MPa)		Elongation (%)	
	930		980		14	

2.3. Experimental setup and procedure

A series of steady-state (isothermal) hot tensile tests were conducted. Tensile tests were carried out using a Zwick/Roell Z100 testing machine (Fig. 4) with maximum load capacity of 100 kN equipped with two separate heating chambers. A three-zone resistance heating furnace, also called high-temperature furnace suitable for testing temperatures from 300 °C to 1300 °C, at a heating rate of ~20 °C/min was used. In this chamber, continuous temperature monitoring was facilitated by means of three N-type thermocouples attached on the upper, central and lower parts of the sample. An environmental chamber was used for temperatures below 300 °C. In this chamber, temperature was measured by one K-type thermocouple attached either on the upper part or lower part of the specimen. Strain measurement of the specimen during tensile testing was accomplished using contact-type extensometers. In environmental chamber, Zwick's "makroXtens" extensometer with extended arms was used while a high-temperature MayTec extensometer with ceramic sensor arms in the three-zone resistance furnace was utilized. Seven different target temperatures were considered: RT, 100 °C, 200 °C, 300 °C, 400 °C, 500 °C, 600 °C, 700 °C, 800 °C and 900 °C. As a testing procedure, the sample was first heated up to its target temperature at a constant heating rate of 20 °C/min after it was mounted and gripped inside the chamber. Prior to loading, the sample was held at the target temperature for 5 min in order to eliminate thermal gradient and ensure uniform temperature. Strain-controlled tensile tests were then conducted with a constant strain rate of 0.0001 s^{-1} until rupture. The testing procedure was similar to those in the literature [6,26,27,33].

3. Results and discussion

In order to study the fire behavior of UHSSs, mechanical properties such as modulus of elasticity, proof stress at different strain levels, ultimate tensile strength and total strain at ultimate tensile strength were determined. Inasmuch as a pronounced yield point is absent in stress-strain curves, assessment of yield strengths at different strain levels has been practiced especially for elevated temperatures as the stress-strain curve becomes highly nonlinear. In this context, EN 1993-1-2 [23] defines the effective yield strength as the strength at 0.2% total strain level ($f_{0.2}$). Other methods for determining effective yield strengths include defining proof stresses at 0.5%, 1.5% and 2% total strain levels, as practiced commonly by researchers [3,4,17,26]. Determining the values of characteristics strengths and strains are illustrated schematically on a typical stress-strain curve in Fig. 5.

As shown in Fig. 5, elastic modulus at the corresponding temperature is calculated based on the tangent of initial linear part of the stress-strain curve in elastic region. The $f_{0.2}$ being used to define yield strength was determined as the intersection point of stress-strain curve with proportional line offset by 0.2% strain level. The strain corresponding to the 0.2% proof stress is termed as proof strain (ε_y). The same approach has been used to determine $f_{0.5}$ by the means of proportional line from the 0.5% strain level. Yield strengths at 1.5% and 2% strain levels, i.e. $f_{1.5}$ and f_2, were determined from the intersection points of stress-strain curves with vertical lines starting at the given strain values. In the same vein, maximum stress level for each temperature at related stress-

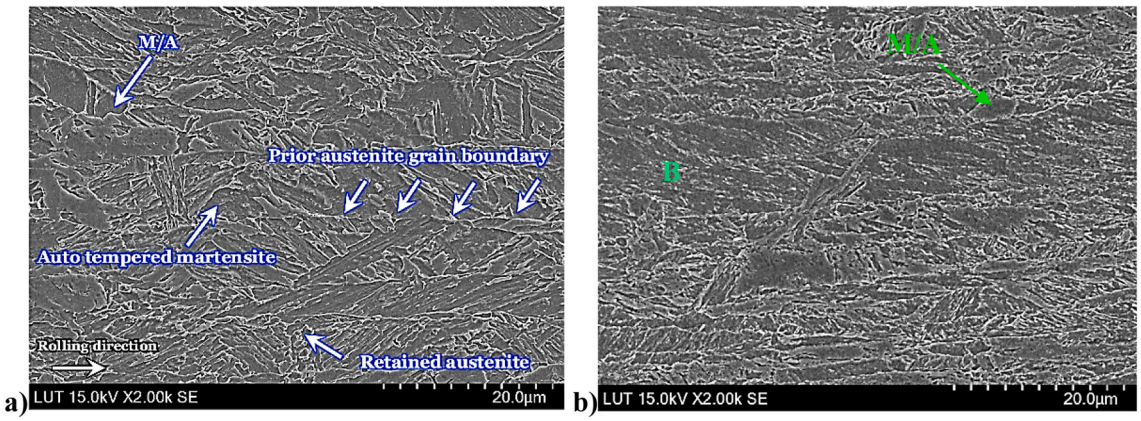

Fig. 1. Scanning electron microscopy of the studied steels, a) S960 [16], b) S1100 [10].

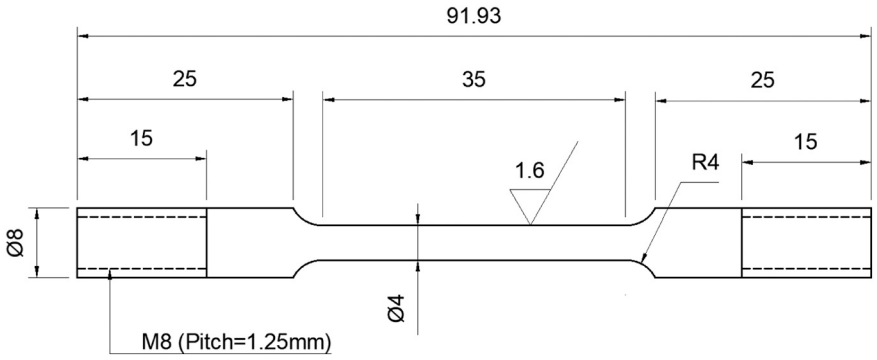

Fig. 2. Schematic of cylindrical specimen used in the study (Dimensions are in mm, not to scale).

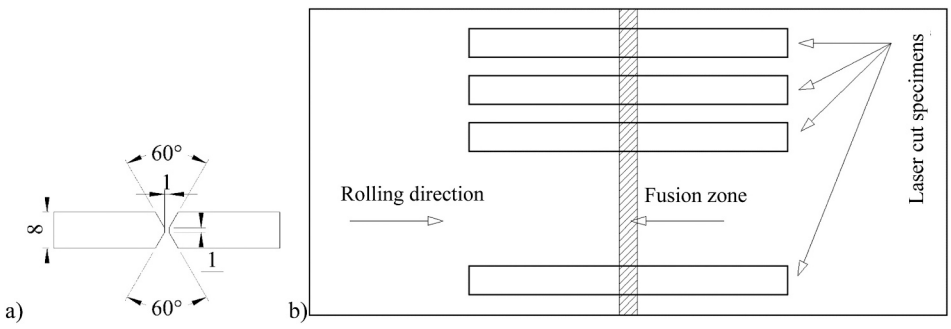

Fig. 3. Specimen preparation, (a) the butt-weld configuration (b) schematic of the butt-welded workpiece and the laser-cut sections. (Dimensions are in mm, not to scale).

strain curve denotes the ultimate tensile strength (f_u), and the corresponding strain level is ultimate total strain or uniform elongation (ε_u).

3.1. Visual observations and failure mode

During the elevated temperature tensile tests, as a general phenomenon, the surface color of the test specimens would change. As can be seen in Fig. 6 (a-d) for both as-received and as-welded specimens made from S960 and S1100, the surface color remains almost silver/white at RT up to 200 °C. When the temperature exceeds 200 °C, the surface color changes slightly to light yellow, and at 300 °C, the color turns to dark blue. From 400 °C to 600 °C, the surface color changes from light gray to almost black. Exceeding 700 °C, the surface color changes to blackish gray due to sever oxidation at those high temperatures and formation of oxide layers [18].

Typical failure mode of tensile test specimens made from as-received and as-welded S960 and S1100 at elevated temperatures are shown in Fig. 6 (a-d). As shown in Fig. 6 (a) and Fig. 6 (c), for all the specimens, both as-received and as-welded, necking occurs before failure, which becomes more obvious as temperature increases. The as-welded S960 specimens fail at the HAZ from RT to 500 °C, as shown in Fig. 6 (b). However, for the same temperature range, all the welded S1100 specimens failed from the BM. Both steel grades revealed a weld failure at 600 °C, followed by irregular failures at higher temperatures.

3.2. Stress-strain curves

The stress-strain curves of as-received and as-welded specimens at RT, as well as various elevated temperatures obtained from steady-state hot tensile tests for S960 and S1100, are plotted in Figs. 7 and 8,

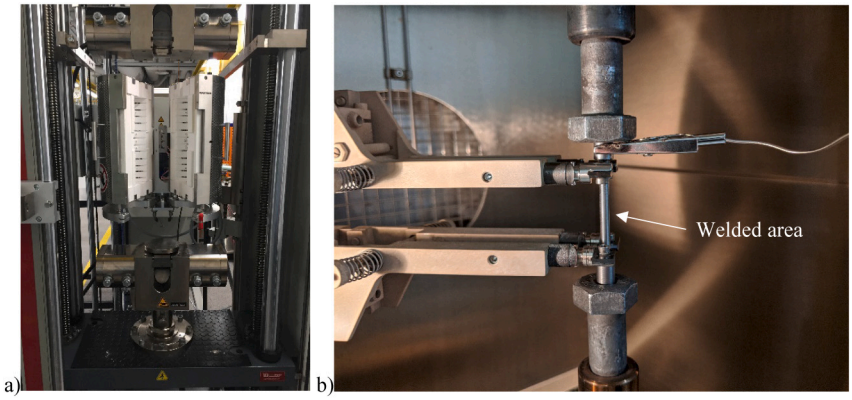

Fig. 4. Tensile testing equipment at elevated temperatures, (a) chamber, (b) round bar specimen.

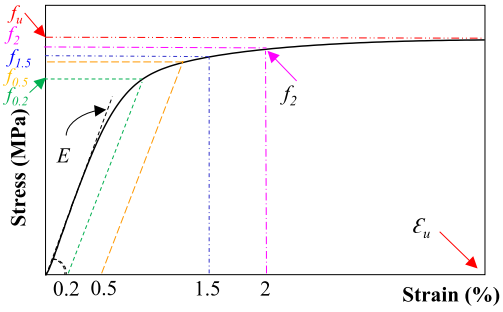

Fig. 5. Schematic of a typical UHSS stress-strain curve up to the ultimate stress and the definition of its characteristics.

respectively. The values corresponding to the characteristic strengths and strains for the examined steel alloys are presented in Tables 5 and 6. It should be mentioned that the abbreviations BM and W corresponds to as-received base material and as-welded conditions, respectively. The numbering in specimen labels 96 and 11 represents the steel grades S960 and S1100, respectively. The testing temperature is added at the end of labeling. For instance, W-96-400 is the butt-welded S960 specimen tested at 400 °C. As can be seen in Figs. 7 and 8, in all the tested cases, as-welded specimen shows smaller ductility compared to the corresponding as-received specimen at the same elevated temperature. Both steel alloys show relatively similar mechanical properties (E, $f_{0.2}$ and f_u) at room temperature. However, the welded joints significantly show different performances. While S960MC shows 35% reduction of its proof stress after being welded, the S1100 revels no reduction, as shown in Fig. 9. As mentioned earlier, softening is attributed to the HAZ of weldments made of UHSSs, which contributes to strength reduction of the joint. A comparison is drawn between the hardness values of the butt-welded joints from S1100 and S960MC. As presented in Fig. 10, both joints in the weld area show comparable hardness with slightly higher values for weldments made of S1100. As moving towards HAZ, while the hardness of welded S1100 reveals no reduction but a fluctuation, there is significant hardness reduction (softening effect) associated with S960MC weldment. Such an effect is correlated to strength reduction of the joints made from S960MC (approximately 35% strength reduction due to welding) as is clear from stress-strain curves in Fig. 9. The hardness reduction at the softened weld HAZ in S960 compared to S1100 is the formation of softer microstructure such as ferrite during the cooling cycle of welding [10].

3.3. Modulus of elasticity

Service performance and load-bearing capacity of steel structures are significantly affected by decrease in elastic modulus at elevated temperatures. A robust fire-resistance design and providing safety to the application of structures made of UHSSs necessitate quantitative evaluation of deterioration of elastic modulus at fire or elevated temperature conditions. In order to discuss the deterioration of elastic modulus with increasing temperature, generally a reduction factor at corresponding temperature is presented. The reduction factor of elastic modulus at a specific elevated temperature is determined as the ratio of elastic modulus at that given temperature to that of RT. Temperature-dependent mechanical properties of steels on the basis of the reduction factor concept is commonly practiced by different design standards, such as Eurocode for fire-resistance design of steel structures [23]. In this study, reduction factors corresponding to elastic modulus at given tested temperatures were obtained from experimental stress-strain curves. A comparison between reduction factors related to elastic modulus (E_T/E_{RT}) for the studied steels (BM and weldment), respective prediction models of design standards (i.e. EC3, AISC and AS4100), and from literature [4,17,26,33] is drawn as shown in Fig. 11. It is essential to mention that reduction factors of elastic modulus for BM-960/1100 in Fig. 11 are calculated as $E_{BM_T}/E_{BM_{RT}}$. In the same vein, reduction factors corresponding to W-960/1100 are $E_{W_T}/E_{W_{RT}}$.

As shown in Fig. 11, the welded joints of both steel alloys show no major reduction in temperature-dependent elastic modulus compared to their BMs. A bilinear curve can be associated with the decrease of elastic modulus for most the data from literature provided for comparison, including BM/W-960, one RT–500 °C, and the other 500 °C–800 °C. The latter has a sharper slope for temperature-induced degradation which is rooted in the elimination of strain hardening at higher temperatures compared to the moderately elevated temperature range RT–500 °C. Elastic modulus of BM/W-1100, although experiencing continuous reduction, compared to BM/W-960, there is lower degradation, and the trend is clearly slower. For example, at 600 °C, while BM/W-960 keeps only 60% of its original elastic modulus, BM/W-1100 retains almost 80% of its elastic modulus at RT. At the same temperature, S460 [33] and S960 [26] lose almost 70% of their elastic modulus at RT. The studied S1100 seems to have a more stable microstructure under temperature gradients resulting less degradation of the mechanical properties. Similar behavior is reported when welded S960 was compared to S1100 at room temperature and after welding [10].

Fig. 11 also indicates that design codes such as EC3, AISC and AS4100 models fairly predict the results of present tests for BM/W-960 in the temperature range RT–300 °C. Predictions of EC3 and AISC in the same manner, start to move on the conservative side as temperature exceeds 300 °C and becomes overly conservative in the temperature range 600 °C–900 °C. The result of the current study up to a temperature of 300 °C agrees with the literature on similar UHSS grades [4,26]. The results of this study in terms of elastic modulus reduction factor values, however, surpass the findings of Qiang et al. [26] and stays below the results of Neuenschwander et al. [4] as temperature increases up to

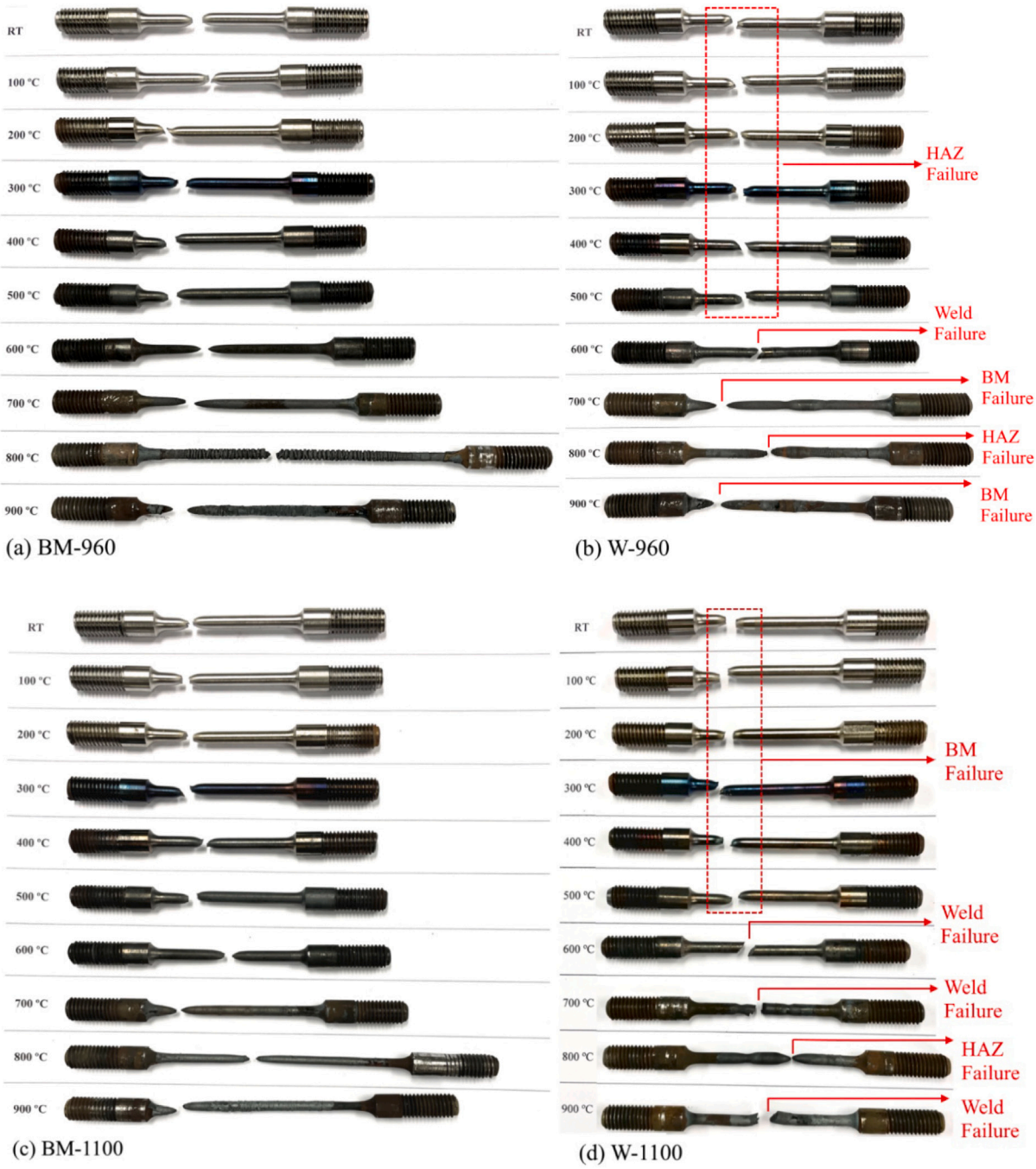

Fig. 6. Visual observation and failure mode of the tested specimen at elevated temperatures, (a) BM-960, (b) W-960, (c) BM-1100, and (d) W-1100.

900 °C. The investigated S960 steel grade in the two mentioned studies was quenched and tempered, while the delivery condition of the S960 in this study was directly quenched. The behavior of S460 is not accurately predicted by EC3 and AISC at temperatures above 300 °C as they become nonconservative and only in the temperature range above 600 °C can reasonably predict the behavior of the material. AS4100 is unsafe for prediction of elastic modulus of S460 at all tested temperatures. All the mentioned design codes are overly conservative regarding the elastic modulus reduction factors of S700 at temperatures 200 °C–400 °C. At temperatures above 400 °C, although the degree of conservativity decreases, EC3 and AISC remain conservative. AS4100 exhibits unsafe prediction at 500 °C for S700 and reasonable predictions in the temperature range 600 °C–800 °C.

The experimental results on the studied BM/W-1100 show a better match with EC3 and AISC models compared to AS4100 for temperatures up to 300 °C as AS4100 leans slightly on the unsafe side. At higher temperatures, all the mentioned design codes are overly conservative for predicting the results of the present test series, with a smaller degree of conservativity for AS4100. Moreover, predications of all the design codes for S1100, compared to S960MC, show more pronounced degrees of conservativity. The results of this study, in terms of elastic modulus of S1100, completely match the data set from the study by Neuenschwander et al. [4], as depicted in Fig. 11.

3.4. Yield strength

Temperature-dependent effective yield strengths of the two tested steels in as-received and as-welded forms based on the reduction factor

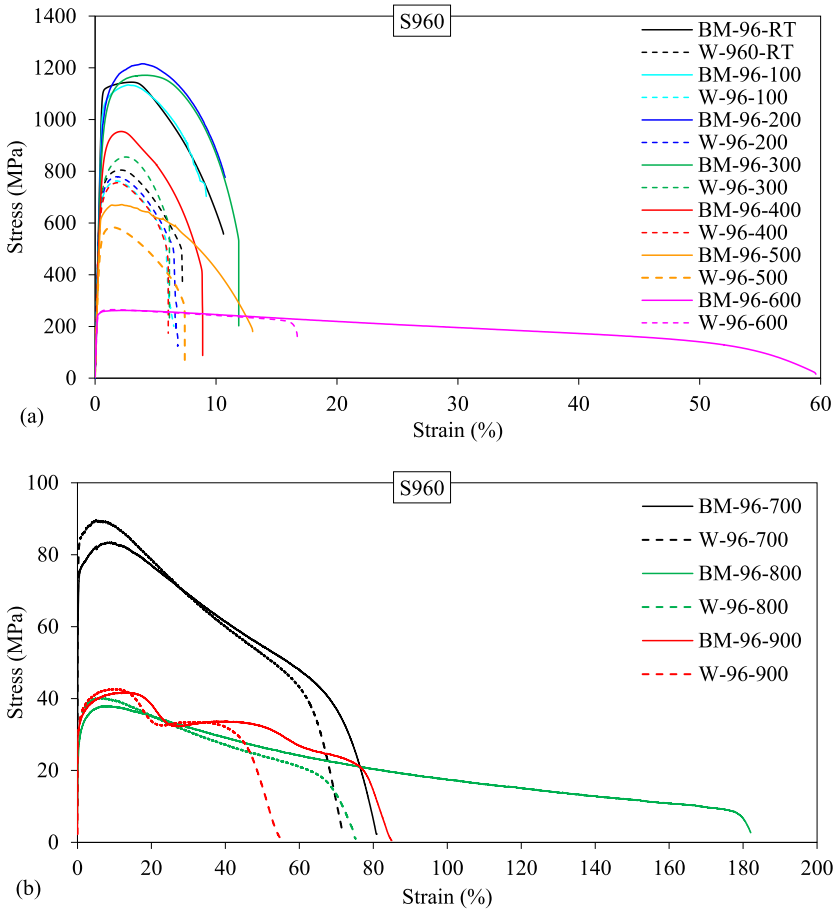

Fig. 7. Engineering stress-strain results of S960 specimens, (a) RT-600 °C, and (b) 700 °C–900 °C.

concept were considered. Effective yield strength reduction factors ($f_{0.2,\ T}/f_{0.2,\ RT}$), ($f_{0.5,\ T}/f_{0.5,\ RT}$), ($f_{1.5,\ T}/f_{1.5,\ RT}$) and ($f_{2,\ T}/f_{2,\ RT}$) corresponding to strain levels 0.2, 0.5, 1.5 and 2, respectively, were calculated as presented in Tables 5 and 6. Reduction factors related to $f_{0.2}$, which is commonly used to define yield strength of the material, are compared with the predictive models from design codes EC3 [23], AISC and AS4100 [32] as well as the literature in Fig. 12. It should be mentioned that reduction factors in Fig. 12 for BM and W are calculated as $f_{0.2BM_T}/f_{0.2BM_{RT}}$ and $f_{0.2W_T}/f_{0.2W_{RT}}$, respectively.

As is shown in Fig. 12, for BM-960, yield strength decreases continuously up to 400 °C, at a lower rate compared to the subsequent temperature range 400 °C–800 °C where significant strength degradation occurs. As is observable in Fig. 12, the same trend of strength reduction is experienced by BM-1100 up to the onset of rapid strength fall at 400 °C. However, compared to BM-960, strength degeneration of BM-1100 at temperatures above 400 °C happens at a slower rate, reaching a reduction factor of almost 0.5 in contrast to 0.2 for BM-960 at 600 °C. Degeneration of $f_{0.2}$ for both BMs continuously continues in a similar manner in the temperature range 700 °C–900 °C.

The absolute 0.2% proof stress of W-960 compared to BM-960 is smaller in the temperature range of RT-600 °C. However, when the reduction factors are compared, the welded S960 shows a better performance. The reason is the significant strength reduction for as-welded joints made of S960 compared to as-received material, as shown in Fig. 9. The strength degradation of BM-960 compared to W-960 at elevated temperatures happens at a greater level and higher rate. Reaching the temperature of 500 °C, W-960 retains 75% of its strength at RT, while such value for BM-960 remains 55%. Significant degradation occurs for both BM/W-960 at 600 °C. The reduction factor for W-960, calculated based on the $f_{0.2}$ at 600 °C to the reference $f_{0.2}$ at RT, takes the value of 0.34, while for the comparable scenario with respect to BM-960, the reduction factor reaches the value of 0.21. Exceeding 600 °C, the values of $f_{0.2}$ for both BM/W-960 becomes quite similar accompanied by significant degradation of strength.

BM-1100 and W-1100 exhibit the same degeneration trend with respect to $f_{0.2}$, such deviation as demonstrated for S960 is not observed. That is, mechanical properties of W-1100 in terms of yield strength can be considered identical to that of BM-1100.

In terms of comparison with design codes, AISC presents the most unsafe predictive model and is inapplicable for HSS/UHSS with respect to $f_{0.2}$. Prediction of reduction factors with respect to $f_{0.2}$ by AISC for S460 is considerably better compared to the rest of the data sets, although in such a scenario, predictions for temperatures above 500 °C remain on the unsafe side. EC3 predictions for BM-960 in the temperature range RT-200 °C is slightly nonconservative, as shown in Fig. 11. Predictions of EC3, however, deviate moderately from experimental data and lean on the conservative side for temperatures up to 500 °C before starting to move into the unsafe region again. For BM-1100, similar overestimation of the yield strength values by EC3 in the temperature range RT-200 °C is demonstrated in Fig. 11. For the rest of the temperature range up to 700 °C, however, EC3 predicts the experimental data with a higher degree of conservativity compared to the data set related to S960. With respect to predictions of EC3 for W-1100, since the experimental data exhibit no significant deviation from the BM-1100 data, predictions of EC3 for W-1100 are similar to predictions for BM-1100. For W-960, the degree of conservativity regarding the predictions of EC3 increases compared to estimations for BM-960. That is, for temperatures RT–100 °C, predictions fall in the unsafe region, while conservative predictions are provided for the entire tested temperatures up to 700 °C before it leans slightly on the unsafe region. Predictions of

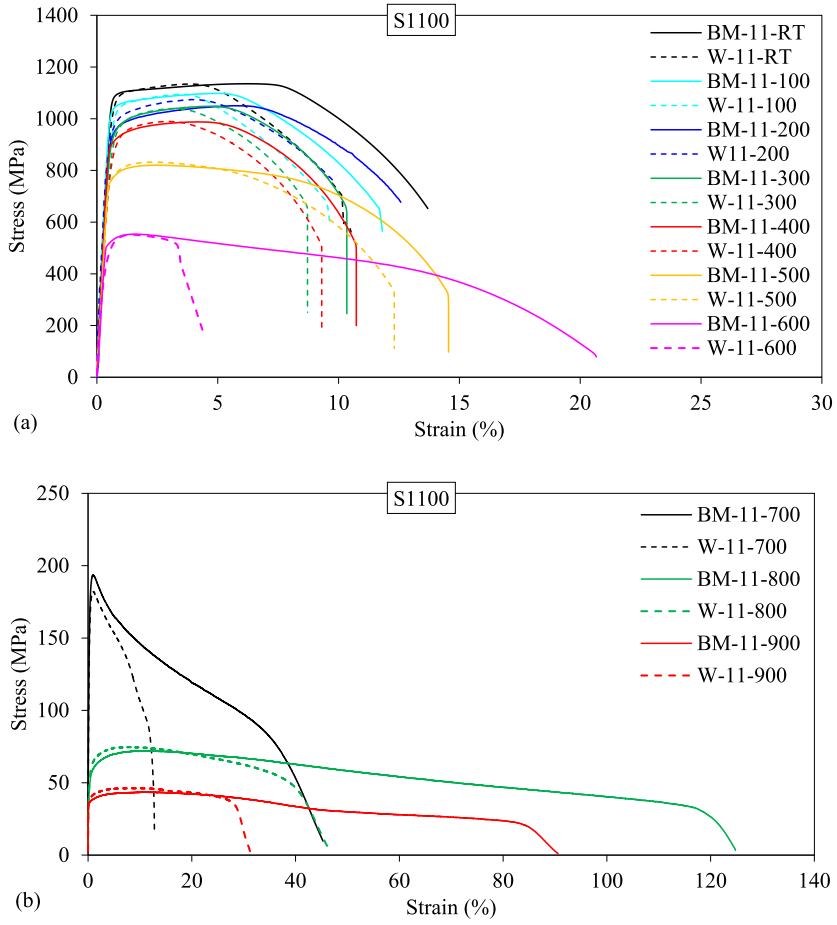

Fig. 8. Engineering stress-strain results of S1100 specimens, (a) RT-600 °C, and (b) 700 °C–900 °C.

Table 5
Mechanical properties of S960 in as-received and as-welded forms at elevated temperatures.

T (°C)	*Label*	*E (GPa)*	$f_{0.2}$*(MPa)*	$f_{0.5}$*(MPa)*	$f_{1.5}$*(MPa)*	f_2*(MPa)*	f_u*(MPa)*	$\varepsilon_{0.2}$	ε_u
RT	BM	199.7	1115.5	1126.9	1133.2	1139.4	1144.6	0.755	3.03
	W	195.4	721.6	764.7	797.5	804.6	804.8	0.574	2.08
100	BM	189.8 (0.95)	1053.5 (0.94)	1083.4 (0.96)	1105.9 (0.97)	1121.5 (0.98)	1134.0 (0.99)	0.752	2.73
	W	183.7 (0.94)	688.5 (0.95)	728.8 (0.95)	759.8 (0.95)	760.6 (0.94)	762.5 (0.95)	0.574	1.77
200	BM	182.1 (0.91)	985.2 (0.88)	1076.3 (0.95)	1143.2 (1.008)	1177.0 (1.033)	1215.7 (1.062)	0.657	3.92
	W	176.4 (0.88)	703.0 (0.97)	747.5 (0.98)	775.9 (0.97)	777.5 (0.97)	778.9 (0.97)	0.602	1.83
300	BM	176.4 (0.88)	949.3 (0.85)	1040.8 (0.92)	1109.4 (0.98)	1140.1 (1.00)	1171.5 (1.02)	0.693	4.13
	W	160.0 (0.82)	721.7 (1.00)	780.7 (1.02)	830.8 (1.04)	849.0 (1.06)	855.3 (1.06)	0.607	2.56
400	BM	164.0 (0.82)	829.3 (0.74)	898.6 (0.80)	941.5 (0.83)	953.3 (0.84)	954.0 (0.83)	0.687	2.18
	W	153.2 (0.78)	655.5 (0.91)	713.5 (0.93)	751.8 (0.94)	755.0 (0.94)	755.8 (0.94)	0.531	1.85
500	BM	144.9 (0.73)	614.0 (0.55)	641.9 (0.57)	668.5 (0.59)	669.6 (0.59)	671.3 (0.59)	0.458	2.20
	W	143.6 (0.73)	523.6 (0.73)	568.0 (0.74)	583.4 (0.73)	577.7 (0.72)	583.6 (0.73)	0.518	1.43
600	BM	113.6 (0.57)	243.8 (0.22)	255.3 (0.23)	261.1 (0.23)	261.7 (0.23)	262.2 (0.23)	0.219	2.63
	W	107.0 (0.55)	248.3 (0.34)	259.8 (0.34)	264.9 (0.33)	264.1 (0.33)	265.0 (0.33)	0.260	2.60
700	BM	80.1 (0.4)	68.7 (0.06)	83.1 (0.07)	85.8 (0.08)	86.3 (0.08)	89.7 (0.08)	0.270	9.17
	W	80.1 (0.41)	78.1 (0.11)	83.1 (0.11)	85.8 (0.11)	86.4 (0.11)	89.7 (0.11)	0.282	5.06
800	BM	42.4 (0.21)	24.1 (0.02)	28.2 (0.03)	32.9 (0.03)	34.1 (0.03)	38.0 (0.03)	0.247	7.32
	W	42.4 (0.22)	29.0 (0.04)	32.7 (0.04)	36.7 (0.05)	37.7 (0.05)	40.1 (0.05)	0.246	6.08
900	BM	62.5 (0.31)	30.4 (0.03)	32.5 (0.03)	35.7 (0.03)	36.6 (0.03)	41.8 (0.04)	0.221	12.16
	W	62.8 (0.32)	30.8 (0.04)	32.9 (0.04)	37.1 (0.05)	38.0 (0.05)	42.7 (0.05)	0.240	9.58

EC3 for W-960 in the temperature range 200 °C –500 °C are overly conservative. AS4100, on the other hand, fails to render accurate predictions for reduction factors of BM/W-1100 up to 300 °C. For the rest of the temperatures, however, this design code provides better agreement with experimental data up to 600 °C. Above 600 °C up to 900 °C, the predictions of AS4100 for BM/W-1100 fall in the unsafe region. With respect to BM-960, AS4100 fails to safely predict reduction factors. For W-960, although the whole prediction package presented by AS4100 is questionable, for temperatures above 200 °C up to 500 °C, safe predictions are provided by such a model. In another comparison between the results of the current study and data sets from the literature [4,26], where BM-960 is concerned, a similar strength degradation trend is observable up to 400 °C. However, between 400 °C and 700 °C, the results of this study show higher strength degradation compared with

Table 6
Mechanical properties of S1100 in as-received and as-welded forms at elevated temperatures.

T (°C)	*Label*	*E (GPa)*	*$f_{0.2}$(MPa)*	*$f_{0.5}$(MPa)*	*$f_{1.5}$(MPa)*	*f_2(MPa)*	*f_u(MPa)*	*$\varepsilon_{0.2}$*	*ε_u*
RT	BM	193.1	1088.9	1102.7	1109.0	1112.8	1135.5	0.759	6.28
	W	192.6	1035.9	1092.9	1108.8	1117.0	1134.3	0.696	3.83
100	BM	192.6 (1.00)	1034.7 (0.95)	1057.5 (0.96)	1069.8 (0.96)	1076.4 (0.97)	1098.3 (0.97)	0.675	5.08
	W	187.2 (0.97)	985.7 (0.95)	1047.6 (0.96)	1067.2 (0.96)	1077.7 (0.96)	1094.4 (0.96)	0.693	3.55
200	BM	189.4 (0.98)	947.1 (0.87)	979.6 (0.89)	999.2 (0.90)	1011.4 (0.91)	1050.5 (0.93)	0.714	5.64
	W	181.9 (0.94)	936.8 (0.90)	997.7 (0.91)	1032.0 (0.93)	1048.1 (0.94)	1074.2 (0.95)	0.599	3.89
300	BM	169.3 (0.88)	942.8 (0.87)	982.6 (0.89)	1007.4 (0.91)	1021.2 (0.92)	1048.5 (0.92)	0.736	4.74
	W	162.9 (0.85)	898.6 (0.87)	971.4 (0.89)	1008.6 (0.91)	1024.2 (0.92)	1039.3 (0.92)	0.684	3.21
400	BM	162.3 (0.84)	889.0 (0.82)	924.4 (0.84)	958.2 (0.86)	969.8 (0.87)	987.9 (0.87)	0.524	4.14
	W	158.9 (0.83)	866.1 (0.84)	937.3 (0.86)	967.2 (0.87)	980.0 (0.88)	989.5 (0.87)	0.703	3.00
500	BM	161.1 (0.83)	745.9 (0.69)	784.2 (0.71)	813.8 (0.73)	819 (0.74)	820.4 (0.72)	0.488	2.47
	W	155.0 (0.80)	741.6 (0.72)	788.1 (0.72)	825.2 (0.74)	831.3 (0.74)	832.2 (0.73)	0.482	2.36
600	BM	143.7 (0.74)	503.0 (0.46)	532.4 (0.48)	553.4 (0.50)	551.8 (0.50)	553.5 (0.49)	0.381	1.59
	W	142.2 (0.74)	468.5 (0.45)	529.5 (0.48)	551.2 (0.50)	545.0 (0.49)	551.3 (0.49)	0.473	1.49
700	BM	121.7 (0.63)	164.6 (0.15)	183.1 (0.17)	190.3 (0.17)	185.7 (0.17)	193.5 (0.17)	0.325	0.92
	W	132.6 (0.69)	152.4 (0.15)	172.5 (0.16)	178.6 (0.16)	174.3 (0.16)	182.1 (0.16)	0.305	0.97
800	BM	44.4 (0.23)	47.1 (0.04)	54.2 (0.05)	62.3 (0.06)	64.3 (0.06)	72.2 (0.06)	0.290	12.15
	W	43.8 (0.23)	51.6 (0.05)	58.6 (0.05)	67.5 (0.06)	69.0 (0.06)	74.8 (0.07)	0.302	8.05
900	BM	66.1 (0.34)	35.9 (0.03)	37.3 (0.03)	39.7 (0.04)	40.3 (0.04)	43.6 (0.04)	0.257	11.21
	W	73.2 (0.38)	38.2 (0.04)	39.9 (0.04)	42.9 (0.04)	43.7 (0.04)	46.4 (0.04)	0.247	7.92

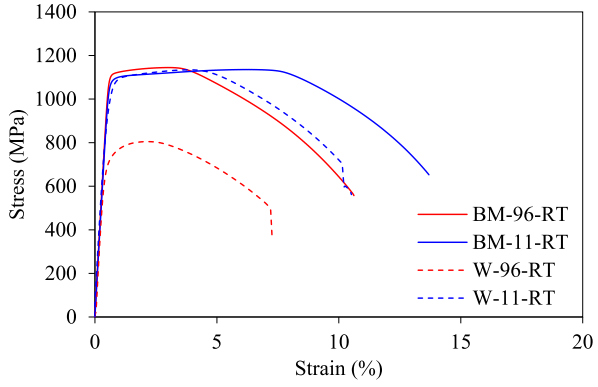

Fig. 9. Engineering stress-strain curves of the base materials and their butt-welds.

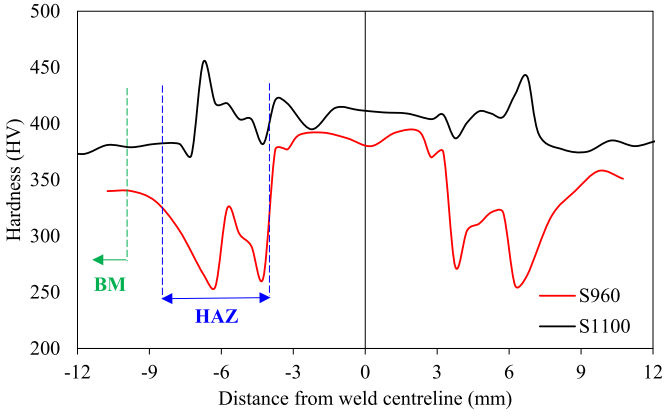

Fig. 10. Vickers hardness distribution along the weldments. (Measurement is performed at the through-thickness 1 mm below surface, modified from [10].)

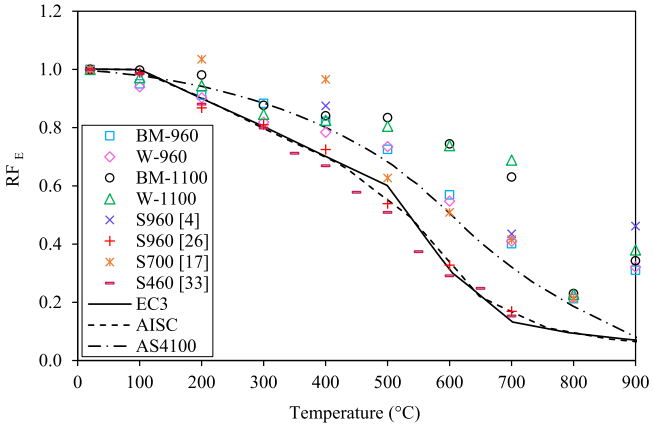

Fig. 11. Elastic modulus reduction factors at elevated temperatures.

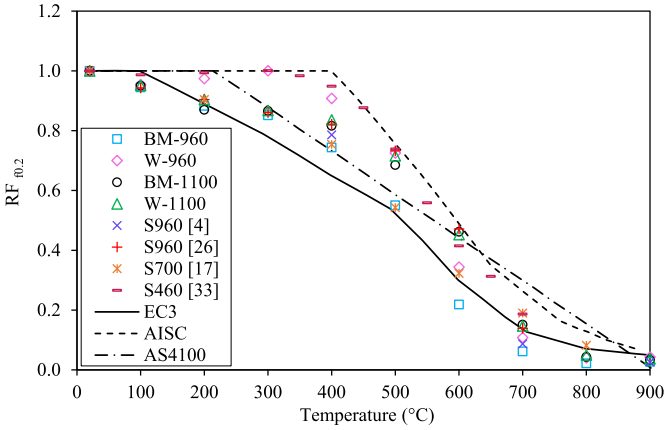

Fig. 12. Reduction factors of 0.2% proof stress at elevated temperatures.

the two studies for S960QL. The reason can be attributed to the higher molybdenum content of S960QL compared to S960MC in this study, almost 0.5% [4] versus 0.125%, respectively, which is believed to increase creep resistance of steels by solid solution strengthening [39]. Compared to S700 from the literature [17], BM-960 keeps the same strength reduction up to around 500 °C before it experiences a more pronounced decline in its strength up to 800 °C. For BM/W-1100, nonetheless, predictions of this study completely match the results of the studies [4,26] in the entire tested temperature range. Experiencing lower deterioration in strength level, the values of reduction factors corresponding to W-960 stand above the reduction factor values of BM/W-1100 and grades above S700 from literature in the temperature range 200 °C–500 °C. Exceeding 500 °C and up to 700 °C, the reduction factor

values of W-960 fall below the corresponding values of BM/W-1100.

3.5. Ultimate tensile strength

The ultimate tensile strength reduction factors of the tested steels as the ratio of ultimate tensile strength at that particular temperature ($f_{u,T}$) to the ultimate tensile strength at RT ($f_{u,RT}$) were calculated, and the results corresponding to BM/W-960 and BM/W-1100 are plotted in Fig. 13. For the purpose of comparison, the predictive models by EC3 and AISC as well data from previous studies related to several HSS/UHSSs are presented.

As depicted in Fig. 13, degeneration of the ultimate tensile strengths of BM/W-960 and BM/W-1100 at elevated temperatures follows the trends which are very close to what was observed for their yield strengths. In this regard, larger reduction factor values at a corresponding temperature for W-960 compared to that of BM-960 is observed for the same reason explained in Section 3.3. For instance, 0.23 versus 0.33, respectively for BM-960 and W-960 at 600 °C. The decline in the ultimate tensile strength of BM-1100 at each corresponding elevated temperature proves to be almost identical to that of W-1100.

Comparing with design codes, the results of ultimate tensile strength reduction factors with respect to BM-960 are an acceptable match with the EC3 predictive model at temperatures up to 500 °C. Prediction of f_u in the range 600 °C–900 °C, however, leans on the unsafe side. Reduction factors of W-960, similar to BM-960, are predicted safely by EC3 in the range RT–500 °C, while between 600 °C and 900 °C estimations tend to be in the unsafe region. At intermediate elevated temperatures, 100 °C–300 °C, stress anomaly is exhibited in the behavior of BM/W-960, with a peak at 200 °C, as was reported in previous studies [7]. While results of this study for S960MC in the temperature range 100 °C–350 °C agree with the EC3 model due to anomaly associated, findings of Neuenschwander et al. [4], and Qiang et al. [26] related to S960QL show a continuous decrease, which makes the EC3 model quite unsafe in the mentioned temperature range for those steels. EC3 is inapplicable to predict the ultimate tensile behavior of S700, while it partially (i.e., temperature range 250 °C–450 °C) can safely predict the ultimate tensile behavior of S460. Having the identical degradation trend, the ultimate tensile behavior of BM/W-1100 at moderately elevated temperatures, 100 °C–350 °C, is inaccurately predicted by the EC3 model. As is revealed, compared to BM/W-960, no stress anomaly is exhibited in the ultimate tensile behavior of BM/W-1100. EC3, however, conservatively estimates the calculated reduction factors for BM/W-1100 at temperatures above 350 °C. Reduction factors of BM/W-1100 predicted by EC3 in the range 700 °C–900 °C tends to match the experimental data. The trend of reduction in the ultimate tensile strength of BM/W-1100 in this study completely matches the findings of the two mentioned studies for S960QL [4,26], which identifies the EC3 model as an unsafe model for the moderately elevated temperature range 100 °C–350 °C.

AISC, on the other hand, predicts reduction factors of BM/W-960 as well as S700 and S460 quite inaccurately, and the degree of safety decreases as temperature rises. Reduction factors related to BM/W-1100 as well as S960QL from a previous study [26] estimated by AISC are in agreement with experimental data only at temperatures above 500 °C and below 650 °C, while the model is inapplicable to safely predict the ultimate tensile behavior of the mentioned steels at temperatures below 500 °C and temperatures above 650 °C.

4. Predictive equations for UHSS

Based on the experimental results of this study for the tested UHSSs including as-received and as-welded, as well as the dataset from the literature for the UHSS grade 960 [4,26] predictive equations are developed as a function of temperature to describe the degradation of the mechanical properties of UHSSs at elevated temperatures. These equations can safely predict mechanical properties reduction factors at elevated temperatures and be thus useful in the field of structural engineering to conduct fire-safe designs for the tested UHSSs.

4.1. Modulus of elasticity

The datasets used to derive the predictive equation for elastic modulus reduction factors of S960 and S1100 are shown in Fig. 14. As can be seen, data scatter increases as temperature rises mainly due to the difference of the elastic modulus values of S960 reported by reference [26]. As is observable, on condition that the data of reference [26] is excluded, the prediction curve may be less conservative in the temperature range 300 °C–800 °C. Mean−2SD was chosen as the criterion to derive the predictive equation, where SD is the standard deviation of the data including the data of the reference [26].

Deterioration of the elastic modulus in the form of reduction factors are presented by Eq. (3).

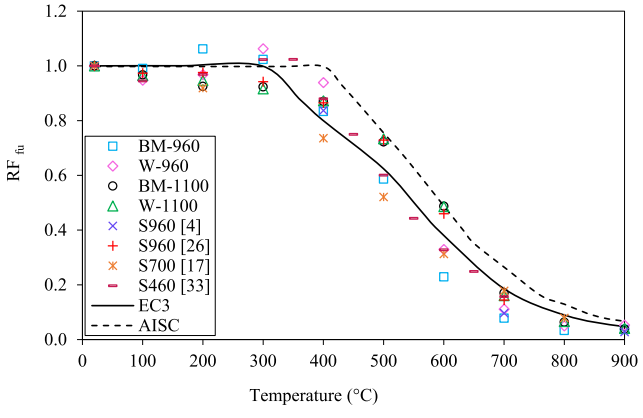

Fig. 13. Reduction factors of f_u at elevated temperatures.

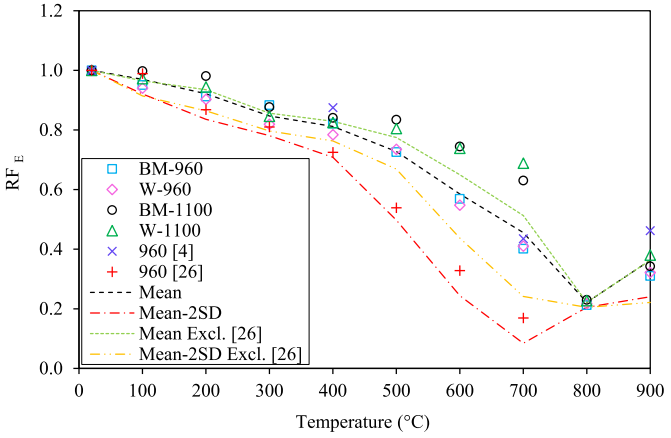

Fig. 14. The dataset used in order to derive the predictive equation for elastic modulus reduction factors of UHSSs.

$$E_T/E_{RT} = \begin{cases} 3\times10^{-9}T^3 - 7\times10^{-8}T^2 - 0.001\times T + 1.0203 \\ 20 \le T < 300 \\ 2\times10^{-11}T^4 - 2\times10^{-8}T^3 - 5\times10^{-6}T^2 + 0.0057\times T - 0.1604 \\ 300 \le T < 700 \\ -4\times10^{-6}T^2 + 0.0076\times T - 3.1406 \\ 700 \le T \le 900 \end{cases} \quad (3)$$

Fig. 15 compares the derived equation for prediction of the elastic modulus reduction factors of UHSSs with some of the design code models.

As is observable in Fig. 15, all the design codes, as it pertains to UHSSs, need to be modified for safer predictions in the temperature range RT–300 °C. in the temperatures range 300 °C–700 °C, the predictive curve becomes close to EC3 and AISC models, albeit with safe predictions of elastic modulus reduction factors for the entire UHSS envelopes used in this study.

4.2. Yield strength

The datasets to derive the yield strength reduction factor relationships of S960 and S1100 are shown in Fig. 16. The same criterion, namely Mean−2SD was used to establish the predictive equation to safely predict the yield strength reduction factors.

The elevated-temperature yield strength reduction factors of UHSSs can be expressed using the following equation:

$$f_{0.2,T}/f_{0.2,RT} = \begin{cases} -6\times10^{-11}T^4 + 5\times10^{-8}T^3 - 10^{-5}T^2 + 0.0004\times T + 0.9972 \\ 20 \le T < 400 \\ -9\times10^{-6}T^2 + 0.0063\times T - 0.3729 \\ 400 \le T < 600 \\ 3\times10^{-6}T^2 - 0.0055\times T + 2.2698 \\ 600 \le T \le 900 \end{cases} \quad (4)$$

A comparison is drawn in Fig. 17 between the predictive equation for the yield strength reduction factors of UHSSs 960 and 1100 and some of the design code models.

As can be observed in Fig. 17, among the design code models, EC3 is closer to the predictive curve developed in this study than other models considering some modifications in the range RT–300 °C and above 600 °C. However, one should consider that EC3 uses mean-2SD value, while the other codes use mean itself in their reliability predictions.

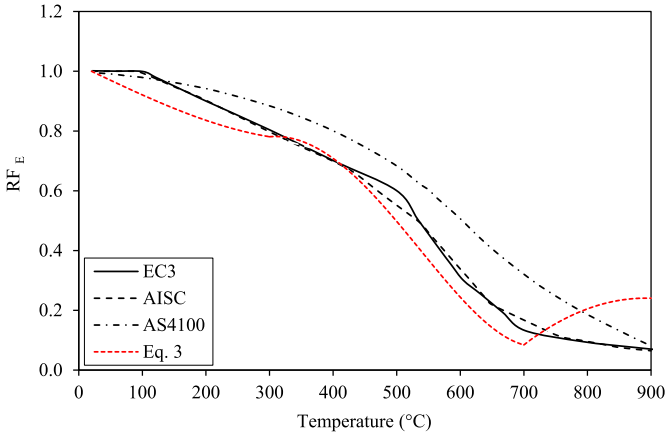

Fig. 15. Comparison between Eq. (3) and design code models.

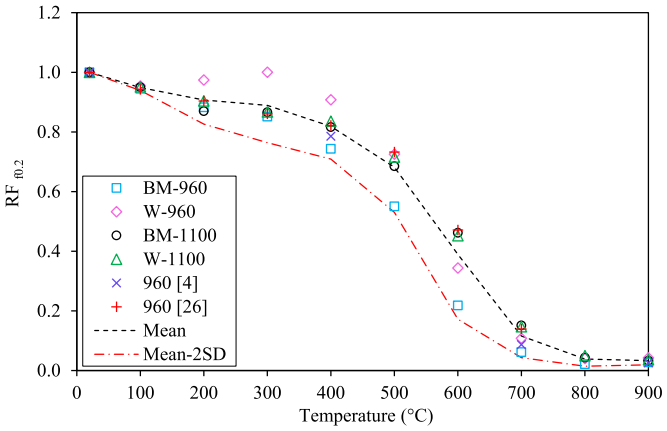

Fig. 16. The dataset used in order to derive the predictive equation for the yield strength reduction factors of UHSSs.

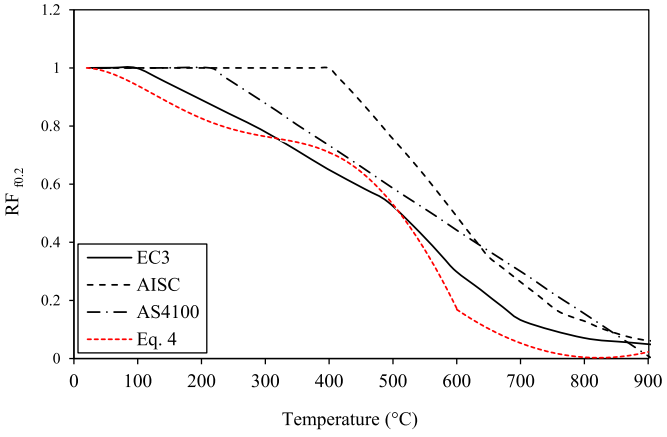

Fig. 17. Comparison between Eq. (4) and design codes models.

4.3. Ultimate tensile strength

In order to derive the equation to predict the ultimate tensile strength reduction factors of UHSSs, the datasets are shown in Fig. 18. As

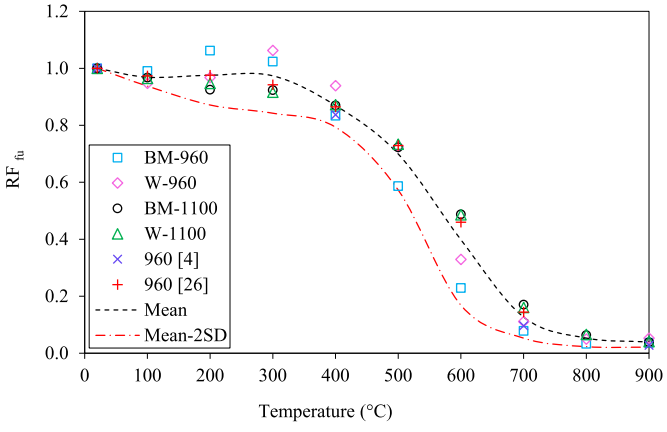

Fig. 18. The dataset used in order to derive the predictive equation for the ultimate tensile strength reduction factors of UHSSs.

is shown, the curve which represents the criterion to derive the equation, namely Mean−2SD can provide safe predictions for the entire UHSS package used in this study.

Degradation of the ultimate tensile strength of the UHSS data envelopes used in this study at elevated temperatures is expressed by the following equation:

$$f_{u,T}/f_{u,RT} = \begin{cases} -4\times10^{-11}T^4+3\times10^{-8}T^3-5\times10^{-6}T^2-0.0004\times T+1.0107 \\ 20\le T<400 \\ -9\times10^{-6}T^2+0.0061\times T-0.1603 \\ 400\le T<600 \\ 3\times10^{-6}T^2-0.0047\times T-1.9841 \\ 600\le T\le900 \end{cases} \quad (5)$$

The proposed equation to estimate the ultimate tensile strength reduction factors of UHSSs in this study is compared with the design code models, as shown in Fig. 19.

As can be seen, in order to predict the ultimate tensile strength reduction factors of UHSSs safely in the entire temperature range RT–900 °C, the predictive model is more conservative than the existing design code models such as EC3 and AISC. Both design code models have obvious unsafe regions between RT and 300 °C, which should be modified in the case of UHSSs.

5. Conclusions

In this study, elevated-temperature mechanical properties of UHSSs grades 960MC and 1100 in both as-received and as-welded forms were examined. Elevated-temperature steady-state tensile tests up to 900 °C were conducted and stress-strain curves, temperature-dependent elastic modulus, 0.2% proof and ultimate tensile strengths were determined. Elastic modulus of as-received S960/1100 with their as-welded forms at all tested temperatures remains almost identical. In terms of 0.2% proof and ultimate tensile strengths, although there is significant welding-induced strength reduction associated with S960MC, elevated-temperature strength reduction with respect to as-welded form surprisingly occurs at a lower level and rate compared to as-received form. S1100 shows no noticeable variation in strength degradation trends for as-received and as-welded forms.

In terms of comparison with several design codes, it can be stated that none of them can be used for accurate prediction of constitutive mechanical behavior of HSS/UHSSs at elevated temperatures and accordingly safe fire-resistance design. All the design codes used in this paper for the sake of comparison, proved to need reconsideration in their predictive models for temperatures below 300 °C for HSS/UHSSs, as they partially but not safely predicted elevated-temperature mechanical properties.

In terms of elastic modulus, for the temperature range above 300 °C, EC3 shows more adaptability to the entire UHSS data package used in this study, while the two other design code models largely underestimate temperature-dependent elastic modulus, and this conservativity increases as temperature and strength level of the material rises. For 0.2% proof strength, AISC is inapplicable for UHSSs, and EC3 surpasses AS4100 in terms of partial adaptability to HSS/UHSSs. In terms of ultimate tensile strength, although applicability of design code models for HSS/UHSSs is questionable, in the temperature range above 300 °C, as steel strength increases, the possibility to adopt EC3 for prediction of mechanical properties increases. Further investigation should be conducted to study in detail the effect of manufacturing process on strength degradation of different grades of UHSSs and their weldments at elevated temperatures. It is also worth including the effect of strain rate on elevated-temperature mechanical properties of UHSSs at higher temperatures, as can happen in real fire situations.

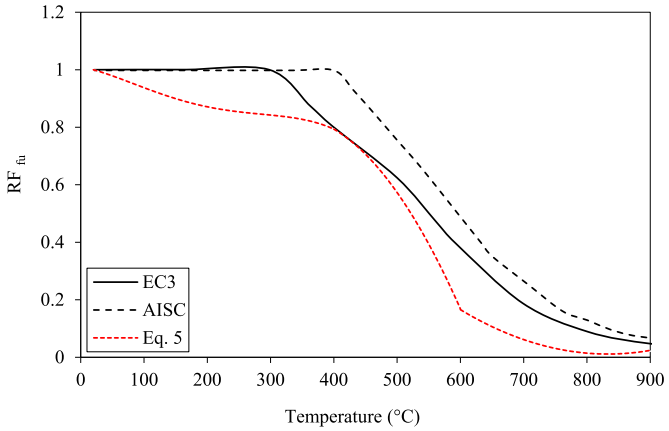

Fig. 19. Comparison between the proposed equation for prediction of the ultimate tensile strength reduction factors and some design code models.

CRediT authorship contribution statement

Mehran Ghafouri: Conceptualization, Methodology, Validation, Investigation, Resources, Writing – original draft, Writing – review & editing, Visualization. **Mohsen Amraei:** Conceptualization, Methodology, Validation, Investigation, Resources, Writing – original draft, Writing – review & editing, Visualization. **Aki-Petteri Pokka:** Methodology, Validation, Investigation, Writing – review & editing. **Timo Björk:** Resources, Supervision, Funding acquisition, Writing – review & editing. **Jari Larkiola:** Resources, Supervision, Writing – review & editing. **Heidi Piili:** Funding acquisition, Writing – review & editing. **Xiao-Lin Zhao:** Conceptualization, Methodology, Supervision, Writing – review & editing.

Declaration of Competing Interest

The authors declare that they have no known competing financial interests or personal relationships that could have appeared to influence the work reported in this paper.

Data availability

No data was used for the research described in the article.

Acknowledgements

The financial support of this research from “Finnish Foundation for Technology Promotion”, and “Business Finland” (BF) through the ISA-LUT project is highly appreciated. The support of SSAB Europe in providing the steel materials for this research is acknowledged. The authors also wish to thank the staff members of the Steel Structures research group at LUT University, and Material Production Engineering of Oulu University for assisting in conducting the experiments.

References

[1] M. Dabiri, M. Isakov, T. Skriko, T. Björk, Experimental fatigue characterization and elasto-plastic finite element analysis of notched specimens made of direct-quenched ultra-high-strength steel, Proc. Inst. Mech. Eng. Part C J. Mech. Eng. Sci. 231 (22) (Nov. 2017) 4209–4226, https://doi.org/10.1177/0954406216661210.

[2] M. Ghafouri, A. Ahola, J. Ahn, T. Björk, Welding-induced stresses and distortion in high-strength steel T-joints: numerical and experimental study, J. Constr. Steel Res. 189 (Feb. 2022), 107088, https://doi.org/10.1016/J.JCSR.2021.107088.

[3] F. Azhari, A. Heidarpour, X.L. Zhao, C.R. Hutchinson, Post-fire mechanical response of ultra-high strength (grade 1200) steel under high temperatures: linking

thermal stability and microstructure, Thin-Walled Struct. 119 (Oct. 2017) 114–125, https://doi.org/10.1016/j.tws.2017.05.030.
[4] M. Neuenschwander, C. Scandella, M. Knobloch, M. Fontana, Modeling elevated-temperature mechanical behavior of high and ultra-high strength steels in structural fire design, Mater. Des. 136 (Dec. 2017) 81–102, https://doi.org/10.1016/j.matdes.2017.09.041.
[5] M. Ghafouri, A. Ahola, J. Ahn, T. Björk, Numerical and experimental investigations on the welding residual stresses and distortions of the short fillet welds in high strength steel plates, Eng. Struct. 260 (Jun. 2022), 114269, https://doi.org/10.1016/J.ENGSTRUCT.2022.114269.
[6] G.Q. Li, L.X. Song, Mechanical properties of TMCP Q690 high strength structural steel at elevated temperatures, Fire Saf. J. 116 (Sep. 2020), 103190, https://doi.org/10.1016/j.firesaf.2020.103190.
[7] M. Ghafouri, J. Ahn, J. Mourujärvi, T. Björk, J. Larkiola, Finite element simulation of welding distortions in ultra-high strength steel S960 MC including comprehensive thermal and solid-state phase transformation models, Eng. Struct. 219 (May) (2020) 110804, https://doi.org/10.1016/j.engstruct.2020.110804.
[8] W. Guo, D. Crowther, J.A. Francis, A. Thompson, Z. Liu, L. Li, Microstructure and mechanical properties of laser welded S960 high strength steel, Mater. Des. 85 (Nov. 2015) 534–548, https://doi.org/10.1016/j.matdes.2015.07.037.
[9] S.P. Chiew, C. Cheng, M.S. Zhao, C.K. Lee, T.C. Fung, Experimental study of welding effect on S690Q high strength steel butt joints, ce/papers 3 (3–4) (Sep. 2019) 701–706, https://doi.org/10.1002/cepa.1124.
[10] M. Amraei, A. Ahola, S. Afkhami, T. Björk, A. Heidarpour, X.L. Zhao, Effects of heat input on the mechanical properties of butt-welded high and ultra-high strength steels, Eng. Struct. 198 (Nov. 2019), 109460, https://doi.org/10.1016/j.engstruct.2019.109460.
[11] W. Guo, L. Li, S. Dong, D. Crowther, A. Thompson, Comparison of microstructure and mechanical properties of ultra-narrow gap laser and gas-metal-arc welded S960 high strength steel, Opt. Lasers Eng. 91 (Apr. 2017) 1–15, https://doi.org/10.1016/j.optlaseng.2016.11.011.
[12] M. Amraei, T. Skriko, T. Björk, X.L. Zhao, Plastic strain characteristics of butt-welded ultra-high strength steel (UHSS), Thin-Walled Struct. 109 (Dec. 2016) 227–241, https://doi.org/10.1016/j.tws.2016.09.024.
[13] F. Farrokhi, J. Siltanen, A. Salminen, Fiber laser welding of direct-quenched ultrahigh strength steels: evaluation of hardness, tensile strength, and toughness properties at subzero temperatures, J. Manuf. Sci. Eng. Trans. ASME 137 (6) (Dec. 2015), https://doi.org/10.1115/1.4030177.
[14] T. Skriko, M. Ghafouri, T. Björk, Fatigue strength of TIG-dressed ultra-high-strength steel fillet weld joints at high stress ratio, Int. J. Fatigue 94 (Jan. 2017) 110–120, https://doi.org/10.1016/j.ijfatigue.2016.09.018.
[15] H. Jiao, X.L. Zhao, A. Lau, Hardness and compressive capacity of longitudinally welded very high strength steel tubes, J. Constr. Steel Res. 114 (Nov. 2015) 405–416, https://doi.org/10.1016/j.jcsr.2015.09.008.
[16] M. Amraei, et al., Mechanical properties and microstructural evaluation of the heat-affected zone in ultra-high strength steels, Thin-Walled Struct. 157 (Dec. 2020), 107072, https://doi.org/10.1016/j.tws.2020.107072.
[17] S. Shakil, W. Lu, J. Puttonen, Experimental studies on mechanical properties of S700 MC steel at elevated temperatures, Fire Saf. J. 116 (Sep. 2020), 103157, https://doi.org/10.1016/j.firesaf.2020.103157.
[18] Y. Li, M. Wang, G. Li, B. Jiang, Mechanical properties of hot-rolled structural steels at elevated temperatures: a review, Fire Saf. J. (Oct. 13, 2020) 103237, https://doi.org/10.1016/j.firesaf.2020.103237. Elsevier Ltd.
[19] M. Garlock, I. Paya-Zaforteza, V. Kodur, L. Gu, Fire hazard in bridges: review, assessment and repair strategies, Eng. Struct. 35 (Feb. 2012) 89–98, https://doi.org/10.1016/j.engstruct.2011.11.002.
[20] F. Azhari, A. Heidarpour, X.L. Zhao, On the use of Bernstain-Bézier functions for modelling the post-fire stress-strain relationship of ultra-high strength steel (grade 1200), Eng. Struct. 175 (Nov. 2018) 605–616, https://doi.org/10.1016/j.engstruct.2018.08.088.
[21] J. Outinen, J. Kesti, P. Mäkeläinen, Fire design model for structural steel S355 based upon transient state tensile test results, J. Constr. Steel Res. 42 (3) (Jun. 1997) 161–169, https://doi.org/10.1016/S0143-974X(97)00018-7.
[22] P. Mäkeläinen, J. Outinen, J. Kesti, Fire design model for structural steel S420M based upon transient-state tensile test results, J. Constr. Steel Res. 48 (1) (Oct. 1998) 47–57, https://doi.org/10.1016/S0143-974X(98)00005-4.
[23] EN 1993-1-2, Eurocode 3: Design of Steel Structures - Part 1–2: General Rules - Structural Fire Design, CEN, Brussels, 2005.
[24] T. Ranawaka, M. Mahendran, Experimental study of the mechanical properties of light gauge cold-formed steels at elevated temperatures, Fire Saf. J. 44 (2) (Feb. 2009) 219–229, https://doi.org/10.1016/j.firesaf.2008.06.006.
[25] F. Azhari, A. Heidarpour, X.L. Zhao, C.R. Hutchinson, Mechanical properties of ultra-high strength (grade 1200) steel tubes under cooling phase of a fire: an experimental investigation, Constr. Build. Mater. 93 (Jul. 2015) 841–850, https://doi.org/10.1016/j.conbuildmat.2015.05.082.
[26] X. Qiang, X. Jiang, F.S.K. Bijlaard, H. Kolstein, Mechanical properties and design recommendations of very high strength steel S960 in fire, Eng. Struct. 112 (Apr. 2016) 60–70, https://doi.org/10.1016/j.engstruct.2016.01.008.
[27] X. Qiang, F.S.K. Bijlaard, H. Kolstein, Post-fire mechanical properties of high strength structural steels S460 and S690, Eng. Struct. 35 (Feb. 2012) 1–10, https://doi.org/10.1016/j.engstruct.2011.11.005.
[28] A. Heidarpour, S. Cevro, Q.Y. Song, X.L. Zhao, Behaviour of stub columns utilising mild-steel plates and VHS tubes under fire, J. Constr. Steel Res. 95 (Apr. 2014) 220–229, https://doi.org/10.1016/j.jcsr.2013.12.007.
[29] W. Wang, Y. Zhang, L. Xu, X. Li, Mechanical properties of high-strength Q960 steel at elevated temperature, Fire Saf. J. 114 (Jun. 2020) 103010, https://doi.org/10.1016/j.firesaf.2020.103010.
[30] L. Keränen, M. Kangaspuoskari, J. Niskanen, Ultrahigh-strength steels at elevated temperatures, J. Constr. Steel Res. 183 (Aug. 2021) 106739, https://doi.org/10.1016/J.JCSR.2021.106739.
[31] Specification for Structural Steel Buildings, ANSI/AISC 360–05, American Institute of Steel Construction, Chicago, 2005.
[32] Steel Structures, AS 4100–1998, Australian Standards, Sydney, 1998.
[33] X. Qiang, F.S.K. Bijlaard, H. Kolstein, Elevated-temperature mechanical properties of high strength structural steel S460N: experimental study and recommendations for fire-resistance design, Fire Saf. J. 55 (Jan. 2013) 15–21, https://doi.org/10.1016/j.firesaf.2012.10.008.
[34] J. Siltanen, S. Tihinen, J. Kömi, Laser and laser gas-metal-arc hybrid welding of 960 MPa direct-quenched structural steel in a butt joint configuration, J. Laser Appl. 27 (S2) (Feb. 2015) S29007, https://doi.org/10.2351/1.4906386.
[35] F. Javidan, A. Heidarpour, X.L. Zhao, C.R. Hutchinson, J. Minkkinen, Effect of weld on the mechanical properties of high strength and ultra-high strength steel tubes in fabricated hybrid sections, Eng. Struct. 118 (Jul. 2016) 16–27, https://doi.org/10.1016/j.engstruct.2016.03.046.
[36] T. Björk, J. Toivonen, T. Nykänen, Capacity of fillet welded joints made of ultra high-strength steel, Weld. World 56 (3–4) (2012) 71–84, https://doi.org/10.1007/BF03321337.
[37] M. Amraei, H. Jiao, X.L. Zhao, L.W. Tong, Fatigue testing of butt-welded high strength square hollow sections strengthened with CFRP, Thin-Walled Struct. 120 (Nov. 2017) 260–268, https://doi.org/10.1016/j.tws.2017.09.004.
[38] Standard Test Methods for Tension Testing of Metallic Materials, ASTM E8 / E8M, American Society for Testing and Materials, Conshohocken, 2013.
[39] M.X. Xiong, J.Y. Richard Liew, Y. Du, Effects of heat-treatment methods on mechanical performance of high-tensile strength steel subject to elevated temperatures, Appl. Fire Eng. - Proc. Int. Conf. Appl. Struct. Fire Eng. ASFE 2017 1 (2–3) (Sep. 2018) 379–384, https://doi.org/10.1201/9781315107202-40.